

Giant thermal Hall conductivity from neutral excitations in the pseudogap phase of cuprates

G. Grissonnanche¹, A. Legros^{1,2}, S. Badoux¹, E. Lefrançois¹, V. Zlatko¹, M. Lizaire¹, F. Laliberté¹, A. Gourgout¹, J.-S. Zhou³, S. Pyon⁴, T. Takayama⁴, H. Takagi⁴, S. Ono⁵, N. Doiron-Leyraud¹, and L. Taillefer^{1,6}

1 Institut quantique, Département de physique & RQMP, Université de Sherbrooke, Sherbrooke, Québec J1K 2R1, Canada

2 SPEC, CEA, CNRS-UMR3680, Université Paris-Saclay, Gif-sur-Yvette Cedex 91191, France

3 Materials Science and Engineering Program, Mechanical Engineering, University of Texas at Austin, Austin, Texas 78712, USA

4 Department of Advanced Materials, University of Tokyo, Kashiwa 277-8561, Japan

5 Central Research Institute of Electric Power Industry, Kanagawa 240-0196, Japan

6 Canadian Institute for Advanced Research, Toronto, Ontario M5G 1Z8, Canada

The nature of the pseudogap phase of cuprates remains a major puzzle.

Although there are indications that this phase breaks various symmetries, there is no consensus on its fundamental nature¹. Although Fermi-surface², transport³ and thermodynamic⁴ signatures of the pseudogap phase are reminiscent of a transition into a phase with antiferromagnetic order^{5,6}, there is no evidence for an associated long-range magnetic order. Here we report measurements of the thermal Hall conductivity κ_{xy} in the normal state of four different cuprates ($\text{La}_{1.6-x}\text{Nd}_{0.4}\text{Sr}_x\text{CuO}_4$, $\text{La}_{1.8-x}\text{Eu}_{0.2}\text{Sr}_x\text{CuO}_4$, $\text{La}_{2-x}\text{Sr}_x\text{CuO}_4$, and $\text{Bi}_2\text{Sr}_{2-x}\text{La}_x\text{CuO}_{6+\delta}$) and show that a large negative κ_{xy} signal is a property of the pseudogap phase, appearing with the onset of that phase at the critical doping p^* . Since it is not due to charge carriers – as it persists when the material becomes an insulator, at low doping – or magnons – as it exists in the absence of magnetic order – or phonons – since skew scattering

is very weak, we attribute this κ_{xy} signal to exotic neutral excitations, presumably with spin chirality⁷. The thermal Hall conductivity in the pseudogap phase of cuprates is reminiscent of that found in insulators with spin-liquid states^{8,9,10}. In the Mott insulator La_2CuO_4 , it attains the highest known magnitude of any insulator¹¹.

Among the different families of unconventional superconductors, magnetism and superconductivity are often in close proximity¹². A notable exception is hole-doped cuprates, where instead superconductivity mostly coexists with the pseudogap phase, an enigmatic state of matter whose nature remains unclear¹. The doping p^* for the onset of the pseudogap phase bears the hallmark of an antiferromagnetic quantum critical point¹³, with a sharp drop in the carrier density n , from $n \sim 1 + p$ above p^* to $n \sim p$ below^{3,14}, a T -linear resistivity¹⁴, and a $\log(1/T)$ specific heat⁴. Yet, there is no evidence for long-range magnetic order appearing at p^* . However, numerical solutions to the Hubbard model have shown that a pseudogap phase can arise from short-range antiferromagnetic correlations¹⁵. It has been argued that an exotic state with topological order can account for such a pseudogap and for the drop in carrier density without breaking translational symmetry¹⁶, but the low-energy excitations of such a state have yet to be detected.

In recent years, the thermal Hall effect has emerged as a powerful probe of magnetic texture and topological excitations in insulators. On the theory side, a non-zero thermal Hall conductivity κ_{xy} was shown to arise even without long-range magnetic order, either from the spin chirality of a paramagnetic state⁷ or from fractionalized (topological) excitations in a spin liquid¹⁷. On the experimental side, a sizable κ_{xy} has been measured in insulators without magnetic order, such as the spin-ice system $\text{Tb}_2\text{Ti}_2\text{O}_7$ (ref. 18) and the spin-liquid systems RuCl_3 (ref. 8), volborthite⁹ and Ca

kapellasite¹⁰.

In cuprates, studies of κ_{xy} have so far been limited to the superconducting state^{19,20,21}, except for the case of $\text{YBa}_2\text{Cu}_3\text{O}_y$ (YBCO) at $p = 0.11$, where κ_{xy} was measured in the field-induced normal state²², which has charge-density-wave order¹³. See Methods for a discussion of this particular case.

Here, we investigate the thermal Hall response of the pseudogap phase via measurements of κ_{xy} in four different cuprate materials – $\text{La}_{2-x}\text{Sr}_x\text{CuO}_4$ (LSCO), $\text{La}_{1.6-x}\text{Nd}_{0.4}\text{Sr}_x\text{CuO}_4$ (Nd-LSCO), $\text{La}_{1.8-x}\text{Eu}_{0.2}\text{Sr}_x\text{CuO}_4$ (Eu-LSCO) and $\text{Bi}_2\text{Sr}_{2-x}\text{La}_x\text{CuO}_{6+\delta}$ (Bi2201) – across a wide doping range, from the overdoped metal at $p = 0.24$ down to the Mott insulator at $p = 0$ (Fig. 1a). The κ_{xy} data reported here are all in the normal state, with superconductivity suppressed by application of a magnetic field normal to the CuO_2 planes.

In Nd-LSCO and Eu-LSCO, the critical doping for the onset of the pseudogap phase is at $p^* = 0.23$ (refs. 4, 13, 14) (Fig. 1a). In Fig. 2a, we plot κ_{xy} / T vs T for Nd-LSCO at $p = 0.24$: κ_{xy} is positive and κ_{xy} / T increases monotonically with decreasing T , tracking closely the electrical Hall conductivity σ_{xy} measured on the same sample, satisfying the Wiedemann-Franz law as $T \rightarrow 0$, namely $\kappa_{xy} / T = L_0 \sigma_{xy}$, where $L_0 = (\pi^2/3)(k_B/e)^2$. The large positive value of σ_{xy} is dictated by the large Fermi surface at $p > p^*$ and its Hall number $n_H \sim 1 + p$ (ref. 14). Clearly, at $p = 0.24$, κ_{xy} is due to charge carriers.

We now turn to dopings immediately below the pseudogap critical point. In Fig. 2b, we plot κ_{xy} / T vs T for Nd-LSCO at $p = 0.20$. We see a qualitatively different behavior, with κ_{xy} becoming negative at low T . As seen in Fig. 3a, this qualitative change occurs immediately below p^* . In Eu-LSCO, the very same change occurs across

p^* (Fig. 3b), from positive κ_{xy} above p^* ($p = 0.24$) to negative κ_{xy} (at low T) below p^* ($p = 0.21$), with essentially identical data to Nd-LSCO at $p = 0.24$ and $p = 0.21$.

The negative κ_{xy} is therefore a property of the pseudogap phase.

We also measured κ_{xy} in Bi2201, a cuprate with a different crystal structure to that of Nd-LSCO and Eu-LSCO, on an overdoped sample of La content $x = 0.2$, with p slightly below p^* (ref. 23). In Fig. 2d, we see that $\kappa_{xy}(T)$ in Bi2201 displays a remarkably similar behavior to that of Nd-LSCO and Eu-LSCO at $p < p^*$. A negative thermal Hall conductivity κ_{xy} at low temperature is therefore a generic property of the pseudogap phase, independent of material. Note that the electrical Hall conductivity σ_{xy} measured on the same samples remains positive down to $T \rightarrow 0$ (Figs. 2b, 2d).

We now move to much lower doping. In Fig. 1b, we see that κ_{xy} / T is still negative at low temperature in Eu-LSCO at $p = 0.08$ and in LSCO at $p = 0.06$, where in both cases σ_{xy} is positive and completely negligible (Figs. 2e, 2f), because the samples are almost electrically insulating at low temperature. This shows that the negative κ_{xy} signal of the pseudogap phase is not due to charge carriers.

Magnons can also be excluded as the source of the negative κ_{xy} . In the phase diagram of Fig. 1a, we delineate in gray the regions where static magnetism is detected by μ SR, whether as incommensurate correlations below T_m or as commensurate Néel order below T_N . We see that in all three materials – Nd-LSCO at $p = 0.20$, Eu-LSCO at $p = 0.08$ and LSCO at $p = 0.06$ – the negative κ_{xy} signal is present well above T_m (Fig. 1), where there is no static magnetism. Moreover, the $\kappa_{xy}(T)$ curve for La_2CuO_4 (Fig. 1b), *i.e.* undoped LSCO with $p = 0$, where there is long-range antiferromagnetic order below ~ 300 K (Fig. 1a), is very similar to the curve for LSCO at $p = 0.06$ (Fig. 1b), where there is no magnetic order above $T \sim 5$ K (Fig. 1a). (See Methods for

further discussion of magnons.) We conclude that magnetic order is not responsible for the negative κ_{xy} signal seen in cuprates at all dopings below p^* , and magnons are ruled out as the relevant excitations.

Phonons can generate a non-zero κ_{xy} signal if they are subject to skew scattering by spins²⁴. Spin scattering will also show up in the longitudinal thermal conductivity κ_{xx} , which is dominated by phonons, in two ways: 1) it reduces the magnitude of κ_{xx} relative to a non-magnetic analog material; 2) it produces a field dependence in κ_{xx} , whose strength is measured by the ratio $[\kappa_{xx}(H) - \kappa_{xx}(0)] / \kappa_{xx}(0)$. Let us compare LSCO ($p = 0.06$) to two insulators with strong spin scattering of phonons (and no magnetic order): $\text{Tb}_2\text{Ti}_2\text{O}_7$ (ref. 18) and $\text{Ba}_3\text{CuSb}_2\text{O}_9$ (ref. 25). In the latter two materials, $\kappa_{xx} / T \sim 25 \text{ mW} / \text{K}^2 \text{ m}$ at $T = 15 \text{ K}$, compared to $\kappa_{xx} / T \sim 300 \text{ mW} / \text{K}^2 \text{ m}$ in LSCO (Extended Data Fig. 1d), a massive reduction due to strong spin scattering (see Methods and Extended Data Fig. 2a). The field dependence of κ_{xx} is correspondingly much weaker in LSCO (Extended Data Fig. 2): $[\kappa_{xx}(H) - \kappa_{xx}(0)] / \kappa_{xx}(0) \sim 0.4 \%$ in LSCO (at $T = 15 \text{ K}$, $H = 15 \text{ T}$), compared to 32 % in $\text{Tb}_2\text{Ti}_2\text{O}_7$ (at $T = 15 \text{ K}$, $H = 8 \text{ T}$) and 5 % in $\text{Ba}_3\text{CuSb}_2\text{O}_9$ (at $T = 5 \text{ K}$, $H = 15 \text{ T}$) (see Table 1). One would therefore expect a much smaller κ_{xy} signal from phonons in LSCO, but in fact κ_{xy} in LSCO is much larger. In absolute terms, $|\kappa_{xy} / T| = 2 \text{ mW} / \text{K}^2 \text{ m}$ in LSCO (Fig. 1b), compared to $\sim 0.08 \text{ mW} / \text{K}^2 \text{ m}$ in $\text{Tb}_2\text{Ti}_2\text{O}_7$ and $\sim 0.002 \text{ mW} / \text{K}^2 \text{ m}$ in $\text{Ba}_3\text{CuSb}_2\text{O}_9$ – so 20 to 1000 times larger. In relative terms, $|\kappa_{xy} / [\kappa_{xx}(H) - \kappa_{xx}(0)]| \sim 1$ in LSCO, compared to ~ 0.01 in $\text{Tb}_2\text{Ti}_2\text{O}_7$ and ~ 0.002 in $\text{Ba}_3\text{CuSb}_2\text{O}_9$ (Table 1) – so 100 to 300 times larger. We conclude that phonons are so weakly scattered by spins that they cannot cause the huge κ_{xy} signal in LSCO at $p = 0.06$ (or Eu-LSCO at $p = 0.08$ or La_2CuO_4).

Moreover, the phonon conductivity in Nd-LSCO shows no indication that strong spin scattering sets in abruptly below p^* , to act as a phonon mechanism for the negative

κ_{xy} signal that suddenly appears below p^* . Indeed, κ_{xx} does not decrease below p^* , on the contrary, it increases (Extended Data Fig. 3), most likely because electron-phonon scattering decreases as the charge carrier density drops. We conclude that phonons are not responsible for the large negative κ_{xy} signal of cuprates that appears suddenly below p^* . (See Methods for further discussion.)

The κ_{xy} signal in the Mott insulator La_2CuO_4 (and in LSCO at $p = 0.06$) is the largest ever seen so far in any insulator. Only multiferroic materials like ferrimagnetic $(\text{Fe,Zn})_2\text{Mo}_3\text{O}_8$ have comparable κ_{xy} values¹¹ (Fig. 4b), thanks to their exceptionally strong lattice-spin coupling. That the underlying mechanism is completely different in cuprates and multiferroics can be seen by the field dependence of κ_{xx} , a direct measure of the lattice-spin coupling, which is ~ 100 times larger in $(\text{Fe,Zn})_2\text{Mo}_3\text{O}_8$ (Fig. 4a).

The large negative κ_{xy} reported here for cuprates is not due to electrons, magnons or phonons. It must come from as yet unidentified neutral excitations. Identifying these excitations will shed new light on the nature of the pseudogap phase. It is instructive to compare cuprates with insulators that are believed to host spin-liquid states. The largest κ_{xy} signal so far in such materials was detected in RuCl_3 (Fig. 4b). In this 2D material, spins on a honeycomb lattice are frustrated and only order (antiferromagnetically) below $T_N = 7$ K. Above T_N , the paramagnetic state is thought to be a spin liquid state described by the Kitaev model¹⁷. In Fig. 4c, we reproduce the data of Hentrich *et al.*²⁶ for κ_{xy} / T vs T in RuCl_3 . Above 100 K, κ_{xy} / T is vanishingly small. Below 100 K, κ_{xy} / T grows gradually with decreasing T down to 20 K or so (and then drops rapidly as T_N is approached). In the regime between 20 K and 100 K, κ_{xy} / T is well described by calculations for the Kitaev model¹⁷, implying that the κ_{xy} signal in RuCl_3 comes from itinerant Majorana fermions – exotic neutral excitations of topological character. This interpretation is supported by the observation²⁷ of a

predicted¹⁷ quantization of the thermal Hall conductivity (at low T when AF order is suppressed by applying a field in the 2D planes). Other spin-liquid candidates, like volborthite⁹ and Ca kapellasite¹⁰, exhibit qualitatively similar $\kappa_{xy}(T)$ (Fig. 4d), suggesting that the gradual growth below ~ 100 K is a general behavior.

In Figs. 4c and 4d, we compare our data on LSCO $p = 0.06$ to the data on RuCl_3 and Ca kapellasite, respectively. There is a tantalizing similarity in the gradual growth below 100 K or so, but there are some differences. First, whereas κ_{xy} is positive in these two spin-liquid candidates, it is negative in cuprates. (This may reflect the particular topological character of the different states.) Secondly, the signal in LSCO is ~ 10 to 25 times larger (Fig. 4). Finally, in LSCO, κ_{xy} / T continues to grow down to the lowest measured temperature – but it may well drop below ~ 5 -10 K.

In summary, the thermal Hall effect in cuprates reveals a hitherto unknown facet of the enigmatic pseudogap phase, reminiscent of a spin liquid. It points to a state with chirality⁷. It will be interesting to see whether models of spin-charge separation²⁸, topological order¹⁶ or current loops²⁹, for example, may be consistent with the giant κ_{xy} signal that appears below p^* .

Acknowledgements. L.T. acknowledges support from the Canadian Institute for Advanced Research (CIFAR) and funding from the Natural Sciences and Engineering Research Council of Canada (NSERC), the Fonds de recherche du Québec - Nature et Technologies (FRQNT), the Canada Foundation for Innovation (CFI), and a Canada Research Chair. This research was undertaken thanks in part to funding from the Canada First Research Excellence Fund. Part of this work was funded by the Gordon and Betty Moore Foundation's EPIQS Initiative (Grant GBMF5306 to L.T.).

J.-S.Z was supported by NSF MRSEC DMR-1720595 in the US.

Author contributions. G.G., A.L., S.B., E.L., V.Z., M.L., F.L., A.G., and N.D.-L. performed the thermal Hall conductivity measurements. G.G., A.L., S.B., E.L., V.Z., M.L., and N.D.-L. performed the electrical Hall conductivity measurements. J.-S.Z. grew the Nd-LSCO single crystals. S.P., T.T., and H.T. grew the Eu-LSCO and LSCO single crystals. S.O. grew the Bi2201 single crystal. G.G., N.D.-L. and L.T. wrote the manuscript, in consultation with all authors. L.T. supervised the project.

Author information. The authors declare no competing financial interest.

Correspondence and requests for materials should be addressed to

G.G. (gael.grissonnanche@usherbrooke.ca) or L.T. (louis.taillefer@usherbrooke.ca).

MAIN FIGURE CAPTIONS

Fig. 1 | Phase diagram and thermal Hall conductivity of cuprates.

a) Temperature-doping phase diagram of Nd-LSCO, Eu-LSCO and LSCO, showing the antiferromagnetic phase below the Néel temperature T_N and the pseudogap phase below T^* (ref. 30), which ends at the critical doping $p^* = 0.23$ for both Nd-LSCO (refs. 4, 13, 14) and Eu-LSCO (ref. 4). For LSCO, $p^* = 0.18$ (refs. 13, 30). Short-range incommensurate spin order occurs below T_m , as measured by μ SR on Nd-LSCO (squares, ref. 31), Eu-LSCO (circles, ref. 32) and LSCO (triangles, ref. 33). The colored vertical strips indicate the temperature range where the thermal Hall conductivity κ_{xy} / T at the corresponding doping decreases towards negative values at low temperature (see panel b). **b)** Thermal Hall conductivity κ_{xy} / T versus temperature in a field $H = 15$ T, for four materials and dopings as indicated, color-coded with the vertical strips in panel a.

Fig. 2 | Thermal and electrical Hall conductivities of four cuprates.

Thermal Hall conductivity κ_{xy} , plotted as κ_{xy} / T (red), and electrical Hall conductivity σ_{xy} , expressed as $L_0\sigma_{xy}$ (blue), where $L_0 = (\pi^2/3)(k_B/e)^2$, as a function of temperature in: **a, b)** Nd-LSCO, **d)** Bi2201, **e)** Eu-LSCO, and **f)** LSCO, at dopings p and fields H as indicated. (For Nd-LSCO $p = 0.20$, σ_{xy} was measured at $H = 33$ T (ref. 14).) In Nd-LSCO at $p = 0.24$, κ_{xy} / T and $L_0 \sigma_{xy}$ are both positive at all temperatures and they track each other, satisfying the Wiedemann-Franz law in the $T = 0$ limit. By contrast, for $p < p^*$ in all four materials, κ_{xy} / T falls to large and negative values at low temperature, whereas $L_0\sigma_{xy}$ remains positive. **c)** Sketch of the thermal Hall measurement (see Methods).

Fig. 3 | Thermal Hall conductivity across the pseudogap critical point p^* .

Thermal Hall conductivity κ_{xy} / T for **a)** Nd-LSCO in $H = 18$ T and **b)** Eu-LSCO in $H = 15$ T, at dopings as indicated, on both sides of the pseudogap critical point $p^* = 0.23$. In both materials, κ_{xy} becomes negative at low temperature when $p < p^*$.

Fig. 4 | Comparison with other insulators, including spin liquid candidates.

a, b) Maximal absolute value of κ_{xy} in various insulators, including the multiferroic ferrimagnet $(\text{Fe,Zn})_2\text{Mo}_3\text{O}_8$ (black diamond; ref. 11) – the previous record holder for the largest $|\kappa_{xy}|$ of any insulator – and the spin-liquid insulator RuCl_3 (green squares; refs. 8, 26) – the previous record holder for the largest $|\kappa_{xy}|$ of any insulator without magnetic order. **a)** Maximal $|\kappa_{xy}|$ as a function of the corresponding value of $[\kappa_{xx}(H) - \kappa_{xx}(0)] / \kappa_{xx}(0)$. **b)** Maximal $|\kappa_{xy}|$ as a function of the corresponding κ_{xx} value, on a log-log plot. The values for all materials are listed in Table 1. We see that La_2CuO_4 and LSCO at $p = 0.06$ have the largest known value of all insulators. **c)** Thermal Hall conductivity κ_{xy} / T versus temperature for LSCO at $p = 0.06$ in $H = 15$ T (red) and RuCl_3 in $H = 16$ T (blue, $\times 10$; from ref. 26). In RuCl_3 , the gradual growth of κ_{xy} / T upon cooling below $T \sim 100$ K is attributed to Majorana fermions, the topological excitations of the Kitaev spin liquid^{8,10,17}. Below $T \sim 20$ K, κ_{xy} / T drops

upon approaching the antiferromagnetic (AF) phase (grey). **d)** Same as in panel c), for the spin-liquid insulator Ca kapellasite (green, $\times 25$; from ref. 10). Although much larger and negative, the κ_{xy} signal in LSCO also comes from neutral excitations in a phase without magnetic order. These comparisons point to a spin-liquid character of the pseudogap phase in cuprates.

Material	κ_{xy}	κ_{xx}	$ \Delta\kappa_{xx} $	$ \Delta\kappa_{xx}/\kappa_{xx} $	T	H	Reference
	mW / K m	W / K m	W / K m		K	T	
La ₂ CuO ₄	- 38.6	12.4	~ 0.06	~ 0.005	20	15	this work
LSCO	- 30.0	5.1	~ 0.02	~ 0.004	15	15	this work
Eu-LSCO	- 13.2	4.5	~ 0.015	~ 0.003	15	15	this work
(Fe,Zn) ₂ Mo ₃ O ₈	24	10	3.2	0.32	30	9	11
Fe ₂ Mo ₃ O ₈	24	9	5	0.55	45	14	11
RuCl ₃	8	15.5	0.62	0.04	20	15	8
RuCl ₃	3.5	8	0.45	0.055	35	16	26
Tb ₂ Ti ₂ O ₇	1.2	0.37	0.12	0.32	15.5	8	18
Ca kapellasite	1.1	0.2	---	---	16	15	10
Lu ₂ V ₂ O ₇	1.0	0.75	---	---	50	9	34
Ba ₃ CuSb ₂ O ₉	0.008	0.07	0.0035	0.05	5	15	25

Table 1 | Thermal Hall conductivity in various insulators.

Maximal value of the thermal Hall conductivity κ_{xy} in various insulators, compared to our three cuprates (La₂CuO₄, LSCO $p = 0.06$, Eu-LSCO $p = 0.08$), measured at the temperature T and field H as indicated: the ferromagnet Lu₂V₂O₇ (ref. 34); the multiferroic ferrimagnets Fe₂Mo₃O₈ and (Fe_{0.875}Zn_{0.125})₂Mo₃O₈ (ref. 11); the spin-ice material Tb₂Ti₂O₇ (ref. 18); and the spin-liquid candidates RuCl₃ (refs. 8,26), Ca kapellasite¹⁰ and Ba₃CuSb₂O₉ (ref. 25). We also list the thermal conductivity κ_{xx} measured at the same temperature, in zero field. The change induced in κ_{xx} by the field, $\Delta\kappa_{xx} = \kappa_{xx}(H) - \kappa_{xx}(0)$, is given in absolute and relative terms.

METHODS

SAMPLES

Nd-LSCO. Single crystals of $\text{La}_{2-y-x}\text{Nd}_y\text{Sr}_x\text{CuO}_4$ (Nd-LSCO) were grown at the University of Texas at Austin using a travelling-float-zone technique, with a Nd content $y = 0.4$ and nominal Sr concentrations $x = 0.20, 0.21, 0.22, 0.23,$ and 0.25 . The hole concentration p is given by $p = x$, with an error bar ± 0.003 , except for the $x = 0.25$ sample, for which the doping is $p = 0.24 \pm 0.005$ (for more details, see ref. 14). The value of T_c , defined as the point of zero resistance, is: $T_c = 15.5, 15, 14.5, 12$ and 11 K for samples with $x = 0.20, 0.21, 0.22, 0.23$ and 0.24 , respectively. The pseudogap critical point in Nd-LSCO is at $p^* = 0.23$ (ref. 14).

Eu-LSCO. Single crystals of $\text{La}_{2-y-x}\text{Eu}_y\text{Sr}_x\text{CuO}_4$ (Eu-LSCO) were grown at the University of Tokyo using a travelling-float-zone technique, with a Eu content $y = 0.2$ and nominal Sr concentrations $x = 0.08, 0.21,$ and 0.24 . The hole concentration p is given by $p = x$, with an error bar of ± 0.005 . The value of T_c , defined as the point of zero resistance, is: $T_c = 3, 14$ and 9 K for samples with $x = 0.08, 0.21$ and 0.24 , respectively. The pseudogap critical point in Eu-LSCO is at $p^* = 0.23$ (ref. 4).

LSCO. Single crystals of $\text{La}_{2-x}\text{Sr}_x\text{CuO}_4$ (LSCO) were grown at the University of Tokyo using a travelling-float-zone technique, with nominal Sr concentrations $x = 0.0$ (*i.e.* La_2CuO_4) and 0.06 . The hole concentration p is given by $p = x$, with an error bar of ± 0.005 . The value of T_c , defined as the point of zero resistance, is: $T_c = 0$ and 5 K for samples with $x = 0.0$ and 0.06 , respectively. The pseudogap critical point in LSCO is at $p^* \sim 0.18$ (ref. 30).

Bi2201. Our single crystal of $\text{Bi}_2\text{Sr}_{2-x}\text{La}_x\text{CuO}_{6+\delta}$ (Bi2201) was grown at CRIEPI in Kanagawa using a travelling-float-zone technique³⁵, with La content $x = 0.2$. The value of T_c , defined as the onset of the drop in magnetization, is: $T_c = 18$ K. Given its x and T_c values, the doping of this overdoped sample is such that $p < p^*$ (ref. 23).

TRANSPORT MEASUREMENTS

Our comparative study of heat and charge transport was performed by measuring the thermal Hall conductivity κ_{xy} and the electrical Hall conductivity σ_{xy} on the same sample, using the same contacts made of silver epoxy H20E annealed at high temperature in oxygen.

Thermal measurements. A constant heat current Q was sent in the basal plane of the single crystal (along x), generating a longitudinal temperature difference $\Delta T_x = T^+ - T^-$ (Fig. 2c). The thermal conductivity along the x axis is given by $\kappa_{xx} = (Q / \Delta T_x) (L / wt)$, where L is the separation (along x) between the two points at which T^+ and T^- are measured, w is the width of the sample (along y) and t its thickness (along z). By applying a magnetic field H along the c axis of the crystal (along z), normal to the CuO_2 planes, one generates a transverse gradient ΔT_y (Fig. 2c). The thermal Hall conductivity is defined as $\kappa_{xy} = -\kappa_{yy} (\Delta T_y / \Delta T_x) (L / w)$, where κ_{yy} is the longitudinal thermal conductivity along the y axis. In this study, we take $\kappa_{yy} = \kappa_{xx}$. The thermal Hall conductivity κ_{xy} of our samples was measured in magnetic fields up to $H = 18$ T. The measurement procedure is described in detail in ref. 22.

Electrical measurements. The longitudinal resistivity ρ_{xx} and Hall resistivity ρ_{xy} were measured in magnetic fields up to 16 T in a Quantum Design PPMS in Sherbrooke. (For Nd-LSCO $p = 0.20$, σ_{xy} was measured at $H = 33$ T (ref. 14).) The measurements were performed using a conventional 6-point configuration with a current excitation of 2 mA, using the same contacts as for the thermal measurements (Fig. 2c). The electrical Hall conductivity σ_{xy} is given by $\sigma_{xy} = \rho_{xy} / (\rho_{xx}^2 + \rho_{xy}^2)$.

FIELD DEPENDENCE OF THE THERMAL HALL CONDUCTIVITY

All of the data reported here were taken in a magnetic field (normal to the CuO_2 planes) large enough to fully suppress superconductivity, and thereby access the normal state of Nd-LSCO, Eu-LSCO, LSCO and Bi2201. Indeed, a field of 15 T is sufficient to do this in all samples presented here, down to at least 5 K. In the normal state, κ_{xy} has an intrinsic field dependence. In Extended Data Fig. 4, we show how κ_{xy} in LSCO $p = 0.06$, where $T_c = 5$ K, depends on magnetic field for $T > T_c$: the linear H dependence of κ_{xy} at high T becomes sub-linear at low T .

THERMAL HALL CONDUCTIVITY IN YBCO

In YBCO at $p = 0.11$, there is huge negative κ_{xy} signal in the field-induced normal state²². In this excellent metal, whose Fermi surface is reconstructed by CDW order into a small electron pocket of high mobility¹³, the electrical Hall conductivity σ_{xy} is equally huge. In fact, the WF law was found to hold, namely $\kappa_{xy} / T = L_0 \sigma_{xy}$ as $T \rightarrow 0$, within error bars of $\pm 15\%$ (ref. 22). In other words, the negative κ_{xy} signal in this case is due

to the charge carriers (*i.e.* to electrons). However, because the $\pm 15\%$ uncertainty corresponds to $\pm 12 \text{ mW} / \text{K}^2 \text{ m}$ (in 27 T), it is impossible to know whether the κ_{xy} signal in YBCO might also contain a contribution of -2 to $-6 \text{ mW} / \text{K}^2 \text{ m}$ from neutral excitations (*i.e.* -1 to $-3 \text{ mW} / \text{K}^2 \text{ m}$ in 15 T; Fig. 1b).

THERMAL HALL SIGNAL FROM MAGNONS

In undoped La_2CuO_4 , magnons have been well characterized by inelastic neutron scattering measurements³⁶. There are two magnon branches, each with its own spin gap, of magnitude 26 K and 58 K, respectively. The thermal conductivity of magnons, κ_{mag} , is therefore thermally activated at $T < 26$ K, so that κ_{mag} decreases exponentially at low T . Hess *et al.* have estimated κ_{mag} in La_2CuO_4 by taking the difference between in-plane and out-of-plane conductivities³⁷. In Extended Data Fig. 5, we see that κ_{mag} / T decreases monotonically as $T \rightarrow 0$ below 150 K.

By contrast, κ_{xy} / T in La_2CuO_4 increases monotonically with decreasing T , all the way down to $T \sim 5$ K (Extended Data Fig. 5), a temperature 5 times smaller than the smallest gap, where there are no thermally excited magnons.

Moreover, when we move up in doping to $p = 0.06$, where AF order is gone and LSCO is in a very different magnetic state (Fig. 1a), without well-defined magnons or a spin gap, $\kappa_{xy}(T)$ is essentially identical to that in La_2CuO_4 (Fig. 1b).

We conclude that magnons are not responsible for the large negative κ_{xy} in cuprates.

THERMAL HALL SIGNAL FROM PHONONS

Phonons can produce a non-zero κ_{xy} signal if they undergo skew scattering by spins^{11,24}. Spin scattering of phonons can be detected through its impact on κ_{xx} . First, it reduces the magnitude of κ_{xx} relative to its value without spin scattering. A good example of this is provided by the insulators $\text{Y}_2\text{Ti}_2\text{O}_7$ and $\text{Tb}_2\text{Ti}_2\text{O}_7$. In non-magnetic $\text{Y}_2\text{Ti}_2\text{O}_7$, $\kappa_{xx}(T)$ is large and typical of phonons in non-magnetic insulators (Extended Data Fig. 2a). In isostructural $\text{Tb}_2\text{Ti}_2\text{O}_7$, which has a large moment on the Tb ion, $\kappa_{xx}(T)$ is massively reduced (Extended Data Fig. 2a), as phonons undergo strong spin scattering. At $T = 15$ K, κ_{xx} is 15 times smaller in $\text{Tb}_2\text{Ti}_2\text{O}_7$.

A second and more direct signature of the spin scattering of phonons is a field dependence of κ_{xx} . In $\text{Tb}_2\text{Ti}_2\text{O}_7$, a field of 8 T causes a 30% reduction in κ_{xx} at $T = 15$ K.

(ref. 18; Fig. 4a, Extended Data Fig. 2b, Table 1). In the multiferroic material $(\text{Fe,Zn})_2\text{Mo}_3\text{O}_8$, where the spin-phonon coupling is known to be very strong, a field of 9 T causes a 32% reduction in κ_{xx} at $T = 30$ K (ref. 11; Fig. 4a, Table 1).

Let us now look for those two signatures in cuprates. First in Nd-LSCO, where the negative κ_{xy} signal is absent at $p = 0.24$ and present at $p = 0.21$, with a magnitude ~ 10 times larger than in $\text{Tb}_2\text{Ti}_2\text{O}_7$. If this very large κ_{xy} signal is due to phonons, then there must be some very strong spin scattering of phonons that appears below $p = 0.24$, which will show up as a massive decrease in κ_{xx} . In Extended Data Fig. 3, we see that there is no decrease of κ_{xx} in going from $p = 0.24$ to $p = 0.21$, on the contrary, κ_{xx} increases.

Secondly, let us look at the field dependence of κ_{xx} in LSCO $p = 0.06$, where the negative κ_{xy} signal is ~ 20 times larger than in $\text{Tb}_2\text{Ti}_2\text{O}_7$, at $T = 15$ K and $H = 8$ T (ref. 18; Extended Data Figs. 2b and 2d, Table 1). In LSCO, the change in κ_{xx} induced by a field of 8 T at $T = 14$ K is no more than 1 % (Extended Data Figs. 1e and 2d), so ~ 20 times smaller than in $\text{Tb}_2\text{Ti}_2\text{O}_7$. In addition to being negligible in size, the H dependence of κ_{xx} in LSCO has the wrong T dependence: $[\kappa_{xx}(15\text{T}) - \kappa_{xx}(1\text{T})] / T$ drops below 30 K, whereas κ_{xy} / T keeps growing monotonically as $T \rightarrow 0$ (Extended Data Fig. 1f).

We conclude that phonons are not responsible for the large negative κ_{xy} in cuprates.

EXTENDED DATA FIGURE CAPTIONS

Extended Data Fig. 1 | Magnetic field dependence of κ_{xx} .

Field dependence of κ_{xx} in Eu-LSCO $p = 0.08$ (top panels) and LSCO $p = 0.06$ (bottom panels), displayed in three ways. **a), d)** κ_{xx} / T vs T at $H = 1$ T (blue) and $H = 15$ T (red). The difference between the two curves is very small, not visible by eye. **b), e)** Change in κ_{xx} with field measured relative to its value at $H = 1$ T, $[\kappa_{xx}(H) - \kappa_{xx}(1\text{ T})]$ vs H , for various temperatures as indicated. **c), f)** Change in κ_{xx} between 15 T and 1 T, plotted as $[\kappa_{xx}(H) - \kappa_{xx}(1\text{ T})] / T$ vs T (blue, right axis), compared to $\kappa_{xy}(15\text{ T}) / T$ vs T (red, left axis). Note how at low T the transverse response grows to be as large, if not larger, than the longitudinal response.

Extended Data Fig. 2 | Comparing cuprates to pyrochlores.

a) Thermal conductivity of two isostructural pyrochlore oxides, plotted as κ_{xx} / T vs T at $H = 0$, namely $\text{Y}_2\text{Ti}_2\text{O}_7$ (red) and $\text{Tb}_2\text{Ti}_2\text{O}_7$ (blue) (from (ref. 38)). The presence of disordered magnetic moments in $\text{Tb}_2\text{Ti}_2\text{O}_7$ produces a strong scattering of phonons, seen as a massive suppression of κ_{xx} (15-fold at $T = 15$ K). **b)** Field dependence of κ_{xx} , plotted as $\Delta\kappa_{xx}(H) / \kappa_{xx}(0)$ vs H , with $\Delta\kappa_{xx} = \kappa_{xx}(H) - \kappa_{xx}(0)$, at $T = 15$ K (blue; ref. 18). The strong effect of field (30% in 8 T) is a direct signature of the strong coupling between phonons and spins in $\text{Tb}_2\text{Ti}_2\text{O}_7$. Also shown is the transverse response in $\text{Tb}_2\text{Ti}_2\text{O}_7$ at $T = 15$ K, plotted as κ_{xy} / T vs H (red; ref. 18). Note that in $\text{Y}_2\text{Ti}_2\text{O}_7$, $\kappa_{xy} = 0$ (ref. 18). **c)** Thermal conductivity of two Nd-LSCO samples, on either side of p^* (red, $p = 0.24$; blue, $p = 0.21$), plotted as κ_{xx} / T vs T at $H = 18$ T. We see that contrary to $\text{Tb}_2\text{Ti}_2\text{O}_7$ (panel a), the appearance of the negative κ_{xy} signal in Nd-LSCO below p^* is not accompanied by a large suppression of κ_{xx} , on the contrary (Extended Data Fig. 3). **d)** Same as in b), for LSCO $p = 0.06$, with the same x -axis and y -axis scales and data taken at (nearly) the same temperature. We see that the situation in LSCO is very different to that found in $\text{Tb}_2\text{Ti}_2\text{O}_7$ (panel b): instead of having a small κ_{xy} and a large $\Delta\kappa_{xx}$ (panel b), we now have a large κ_{xy} and a small $\Delta\kappa_{xx}$. Quantitatively, $\kappa_{xy} / \Delta\kappa_{xx} \sim 1$ in LSCO and ~ 0.01 in $\text{Tb}_2\text{Ti}_2\text{O}_7$, at $T = 15$ K and $H = 8$ T (Table 1).

Extended Data Fig. 3 | Change in phonon κ_{xx} across p^* in Nd-LSCO.

a) Thermal conductivity of Nd-LSCO at four different dopings, above p^* ($p = 0.24$) and below p^* ($p = 0.20, 0.21, 0.22$), plotted as κ_{xx} / T vs T , at $H = 18$ T. We see that κ_{xx} increases below p^* . **b)** Same as in panel a), for Nd-LSCO $p = 0.21$ (blue; $H = 18$ T) and LSCO $p = 0.06$ (green, $H = 16$ T). We see that κ_{xx} continues to increase as we lower p further. This shows that phonons conduct better at lower p . A natural explanation is that they are less scattered by charge carriers as the material becomes less metallic. **c)** Same data as in panel a), for Nd-LSCO $p = 0.21$ (blue) and $p = 0.24$ (red), compared to the electrical conductivity of those same samples, plotted as L_0 / ρ vs T (lines; measured at $H = 33$ T (ref. 14)). The latter curves are a reasonable estimate of the electronic thermal conductivity κ_{xx}^{el} , exact at $T \rightarrow 0$ (since the WF law is satisfied³⁹), as seen in Fig. 2a. **d)** Estimate of the phonon conductivity, defined as $\kappa_{xx}^{\text{ph}} = \kappa_{xx} - L_0 / \rho$, plotted as $\kappa_{xx}^{\text{ph}} / T$ vs T (using data in panel c). We see that $\kappa_{xx}^{\text{ph}}(T)$ increases upon crossing below p^* , most probably because electron-phonon scattering is weakened by the loss of carrier

density. There is no evidence that the phonons suddenly suffer from the onset of strong spin scattering below p^* (which would cause $\kappa_{xx}^{\text{ph}}(T)$ to drop below p^*), such as would be required to explain the appearance of the negative κ_{xy} signal below p^* (Fig. 3) as being due to phonon transport.

Extended Data Fig. 4 | Magnetic field dependence of κ_{xy} in LSCO.

a) Field dependence of the thermal Hall conductivity of LSCO at $p = 0.06$, plotted as κ_{xy} vs H at various temperatures, as indicated. The dependence of κ_{xy} on H is linear at high T and it becomes sublinear at lower T . **b)** Deviation from linearity displayed by plotting $\kappa_{xy} / (TH)$ vs T at four different fields, as indicated.

Extended Data Fig. 5 | Magnon thermal conductivity in La_2CuO_4 .

a) Thermal conductivity of magnons in La_2CuO_4 , plotted as κ_{mag} / T vs T (blue, right axis; ref. 37). The solid line is a fit to the data using the standard calculation for two magnon branches in 2D, with gaps as measured by neutron inelastic scattering³⁶, namely $\Delta_1 = 26$ K and $\Delta_2 = 58$ K. Below $T \sim 5$ K, thermally-excited magnons are exponentially rare and $\kappa_{\text{mag}} / T \sim 0$. In sharp contrast, the thermal Hall conductivity of La_2CuO_4 , $|\kappa_{xy} / T|$ (red, left axis; Fig. 1b), is largest at $T \sim 5$ K. This comparison shows that the κ_{xy} signal in La_2CuO_4 cannot come from magnon transport.

¹ Keimer, B. *et al.* From quantum matter to high-temperature superconductivity in copper oxides. *Nature* **518**, 179-186 (2015).

² Fujita, K. *et al.* Simultaneous transitions in cuprate momentum-space topology and electronic symmetry breaking. *Science* **344**, 612-616 (2014).

³ Badoux, S. *et al.* Change of carrier density at the pseudogap critical point of a cuprate superconductor. *Nature* **531**, 201-214 (2016).

⁴ Michon, B. *et al.* Thermodynamic signatures of quantum criticality in cuprate superconductors. *Nature* (in press); arXiv:1804.08502 (2018).

- ⁵ Storey, J. Hall effect and Fermi-surface reconstruction via electron pockets in the high- T_c cuprates. *Europhys. Lett.* **113**, 27003 (2016).
- ⁶ Chatterjee, S., Sachdev, S. & Eberlein, A. Thermal and electrical transport in metals and superconductors across antiferromagnetic and topological quantum transitions. *Phys. Rev. B* **96**, 075103 (2017).
- ⁷ Lee, H., Han, J. H. & Lee, P. A. Thermal Hall effect of spins in a paramagnet. *Phys. Rev. B* **91**, 125413 (2015).
- ⁸ Kasahara, Y. *et al.* Unusual thermal Hall effect in the Kitaev spin liquid candidate α - RuCl_3 . *Phys. Rev. Lett.* **120**, 217205 (2018).
- ⁹ Watanabe, D. *et al.* Emergence of nontrivial magnetic excitations in a spin-liquid state of kagomé volborthite. *PNAS* **113**, 8653 (2016).
- ¹⁰ Doki, H. *et al.* Spin thermal Hall conductivity of a Kagome antiferromagnet. *Phys. Rev. Lett.* **121**, 097203 (2018).
- ¹¹ Ideue, T. *et al.* Giant thermal Hall effect in multiferroics. *Nature Mat.* **16**, 797-802 (2017).
- ¹² Monthoux, P., Pines, D. & Lonzarich, G. G. Superconductivity without phonons. *Nature* **450**, 1177-1183 (2007).
- ¹³ Proust, C. & Taillefer, L. The remarkable underlying ground states of cuprate superconductors. *Annu. Rev. Condens. Matter* (in press); arXiv:1807.05074 (2018).
- ¹⁴ Collignon, C. *et al.* Fermi-surface transformation across the pseudogap critical point of the cuprate superconductor $\text{La}_{2-x}\text{Nd}_{0.4}\text{Sr}_x\text{CuO}_4$. *Phys. Rev. B* **95**, 224517 (2017).
- ¹⁵ Kyung, B. *et al.* Pseudogap induced by short-range spin correlations in a doped Mott insulator. *Phys. Rev. B* **73**, 165114 (2006).

- ¹⁶ Scheurer, M. S. *et al.* Topological order in the pseudogap metal. *PNAS* **115**, E3665-E3672 (2018).
- ¹⁷ Nasu, J., Yoshitake, J. & Motome, Y. Thermal Transport in the Kitaev Model. *Phys. Rev. Lett.* **119**, 127204 (2017).
- ¹⁸ Hirschberger, M. *et al.* Large thermal Hall conductivity of neutral spin excitations in a frustrated quantum magnet. *Science* **348**, 106–109 (2015).
- ¹⁹ Zhang, Y. *et al.* Giant enhancement of the thermal Hall conductivity κ_{xy} in the superconductor $\text{YBa}_2\text{Cu}_3\text{O}_7$. *Phys. Rev. Lett.* **86**, 890–893 (2001).
- ²⁰ Durst, A. C., Vishwanath, A. & Lee, P. A. Weak-field thermal Hall conductivity in the mixed state of *d*-wave superconductors. *Phys. Rev. Lett.* **90**, 187002 (2003).
- ²¹ Cvetkovic, V. & Vafeek, O. Berry phases and the intrinsic thermal Hall effect in high-temperature cuprate superconductors. *Nat. Comm.* **6**, 6518 (2015).
- ²² Grissonnanche, G. *et al.* Wiedemann-Franz law in the underdoped cuprate superconductor YBCO. *Phys. Rev. B* **93**, 064513 (2016).
- ²³ Kawasaki, S. *et al.* Carrier-concentration dependence of the pseudogap ground state of superconducting $\text{Bi}_2\text{Sr}_{2-x}\text{La}_x\text{CuO}_6$ revealed by $^{63,65}\text{Cu}$ -nuclear magnetic resonance in very high magnetic fields. *Phys. Rev. Lett.* **105**, 137002 (2010).
- ²⁴ Strohm, C., Rikken, G. L. J. A. & Wyder, P. Phenomenological evidence for the phonon Hall effect. *Phys. Rev. Lett.* **95**, 155901 (2005).
- ²⁵ Sugii, K. *et al.* Thermal Hall effect in a spin-phonon glass $\text{Ba}_3\text{CuSb}_2\text{O}_9$. *Phys. Rev. Lett.* **118**, 145902 (2017).
- ²⁶ Hentrich, R. *et al.* Large thermal Hall effect in $\alpha\text{-RuCl}_3$: Evidence for heat transport by Kitaev-Heisenberg paramagnons. arXiv:1803.08162 (2018).

- ²⁷ Kasahara, Y. *et al.* Majorana quantization and half-integer thermal quantum Hall effect in a Kitaev spin liquid. *Nature* **559**, 227-231 (2018).
- ²⁸ Kivelson, S. A., Rokhsar, D. S. & Sethna, J. P. Topology of the resonating valence-bond state: Solitons and high- T_c superconductivity. *Phys. Rev. B* **35**, 8865-8868 (1987).
- ²⁹ Varma, C. M. Theory of the pseudogap state of the cuprates. *Phys. Rev. B* **73**, 155113 (2006).
- ³⁰ Cyr-Choinière, O. *et al.* Pseudogap temperature T^* of cuprate superconductors from the Nernst effect. *Phys. Rev. B* **97**, 064502 (2018).
- ³¹ Nachumi, B. *et al.* Muon spin relaxation study of the stripe phase order in $\text{La}_{1.6-x}\text{Nd}_{0.4}\text{Sr}_x\text{CuO}_4$ and related 214 cuprates. *Phys. Rev. B* **58**, 8760–8772 (1998).
- ³² Klauss, H.-H. *et al.* From antiferromagnetic order to static magnetic stripes: the phase diagram of $(\text{La, Eu})_{2-x}\text{Sr}_x\text{CuO}_4$. *Phys. Rev. Lett.* **85**, 4590–4593 (2000).
- ³³ Hücker, M. *et al.* Coupling of stripes to lattice distortions in cuprates and nickelates. *Physica C: Superconductivity and its Applications* **460–462**, 170–173 (2007).
- ³⁴ Onose, Y. *et al.* Observation of the magnon Hall effect. *Science* **329**, 297–299 (2010).
- ³⁵ Ono, S. & Ando, Y. Evolution of the resistivity anisotropy in $\text{Bi}_2\text{Sr}_{2-x}\text{La}_x\text{CuO}_{6+\delta}$ single crystals for a wide range of hole doping. *Phys. Rev. B* **67**, 104512 (2003).
- ³⁶ Keimer, B. *et al.* Soft phonon behavior and magnetism at the low temperature structural phase transition of $\text{La}_{1.65}\text{Nd}_{0.35}\text{CuO}_4$. *Z. Phys. B* **91**, 373 (1993).
- ³⁷ Hess, C. *et al.* Magnon heat transport in doped La_2CuO_4 . *Phys. Rev. Lett.* **90**, 197002 (2003).
- ³⁸ Li, Q. J. *et al.* Phonon-glass-like behavior of magnetic origin in single crystal $\text{Tb}_2\text{Ti}_2\text{O}_7$. *Phys. Rev. B* **87**, 214408 (2013).

³⁹ Michon, B. *et al.* Wiedemann-Franz law and abrupt change in conductivity across the pseudogap critical point of a cuprate superconductor. *Phys. Rev. X* **8**, 041010 (2018).

Figure 1

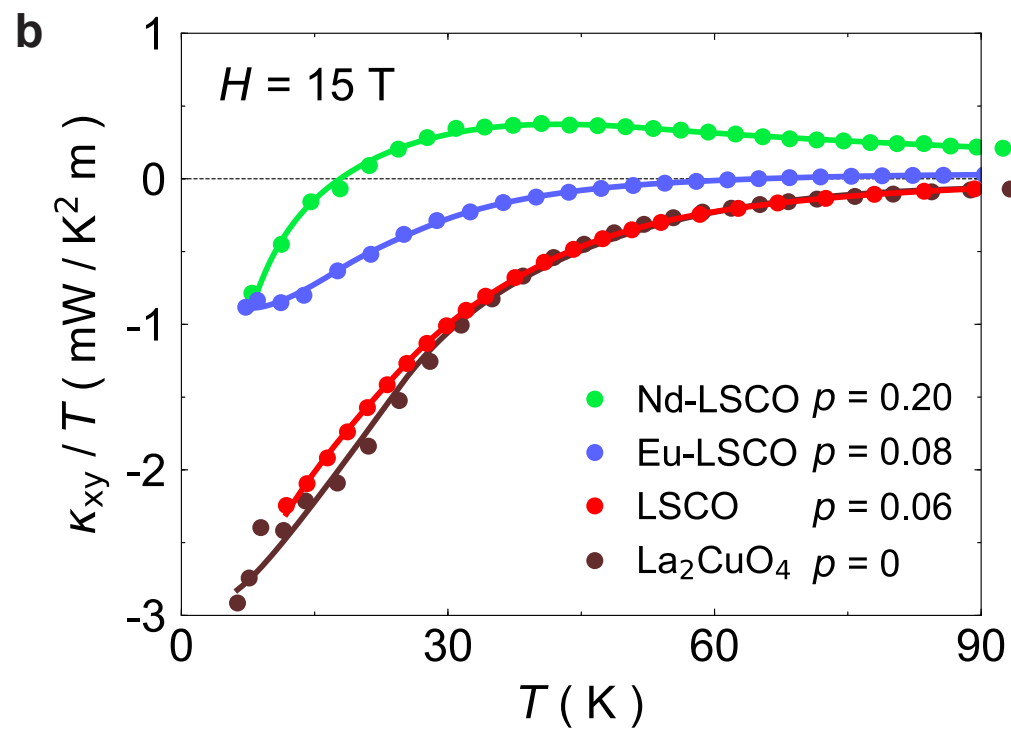
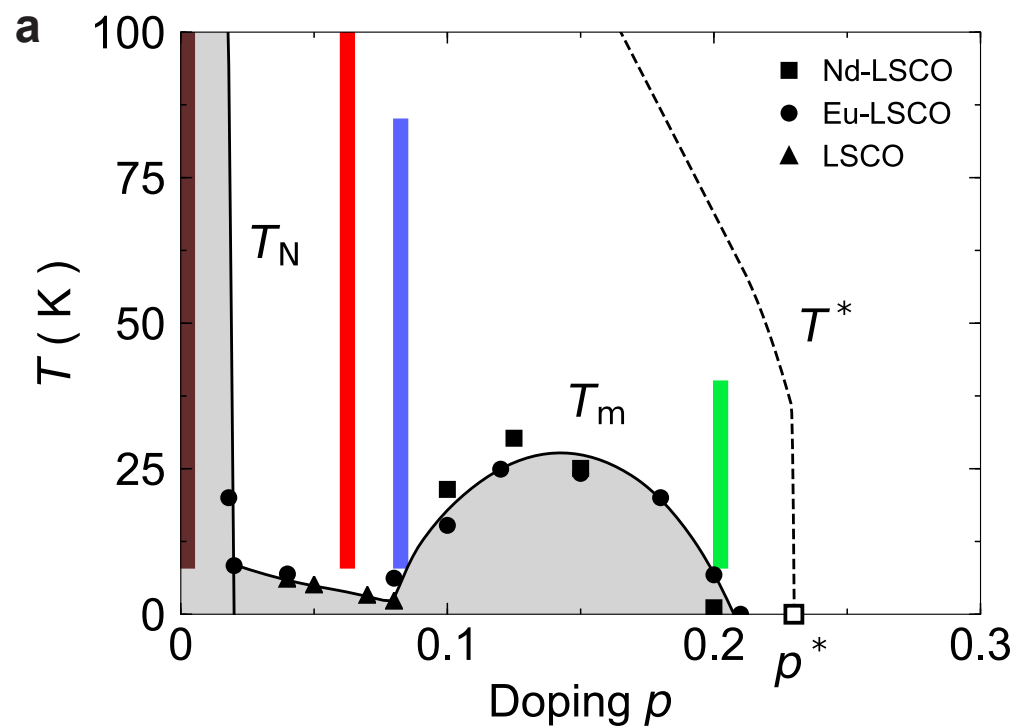


Figure 2

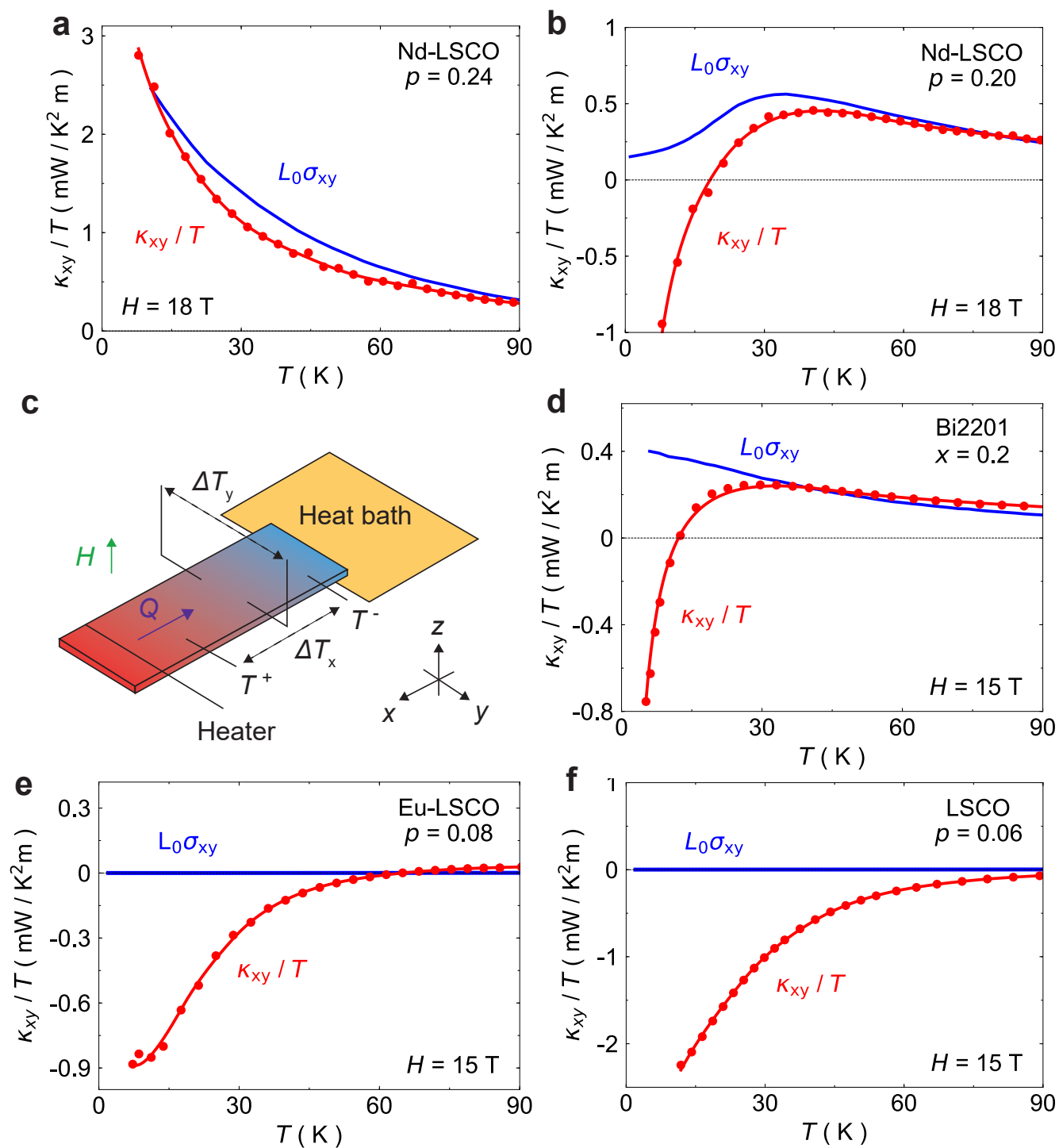


Figure 3

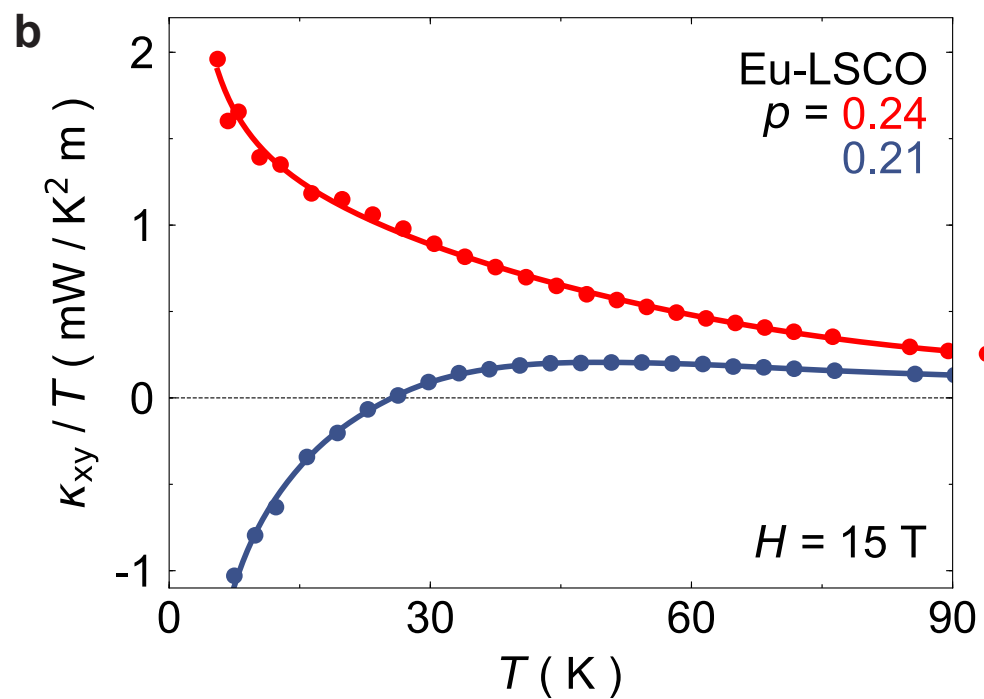
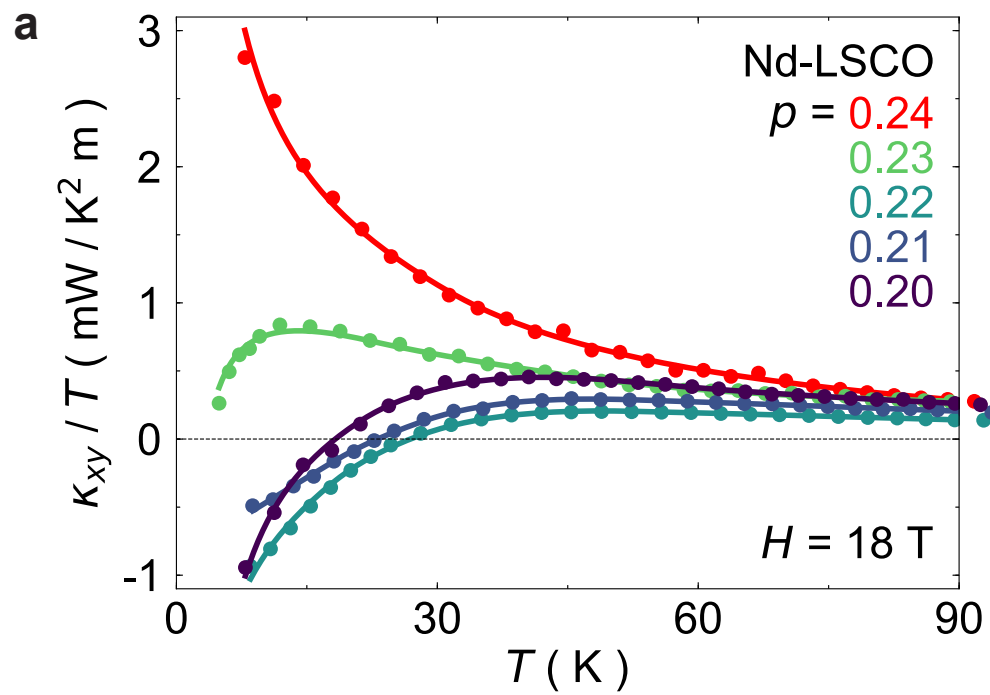
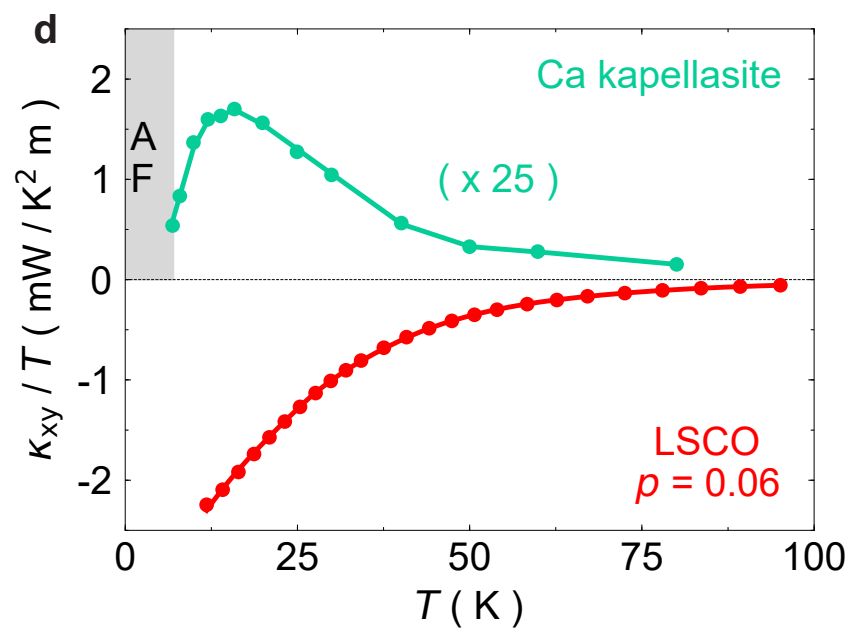
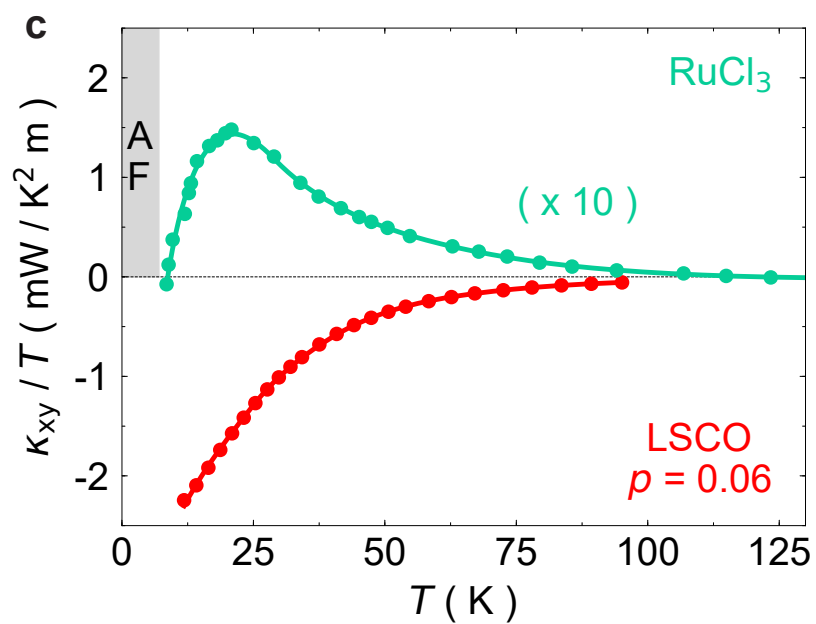
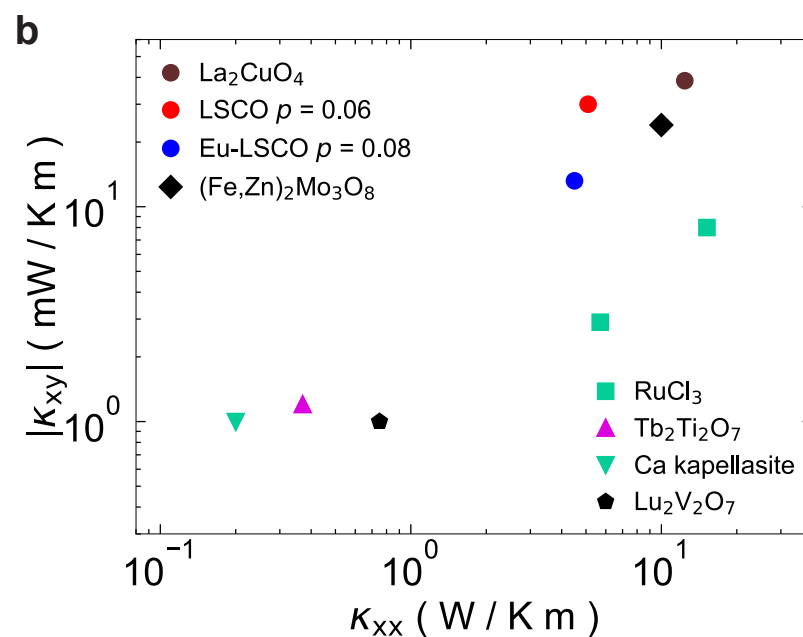
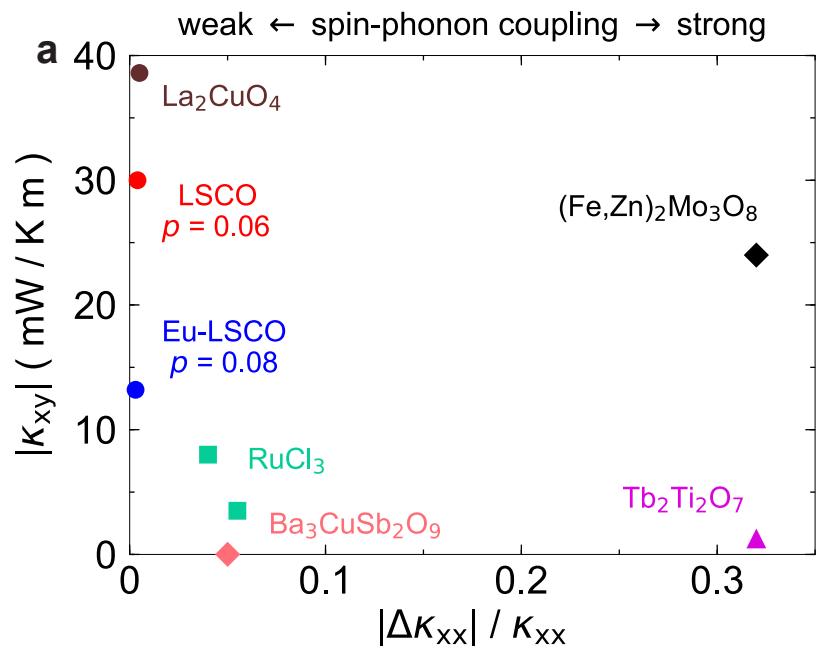
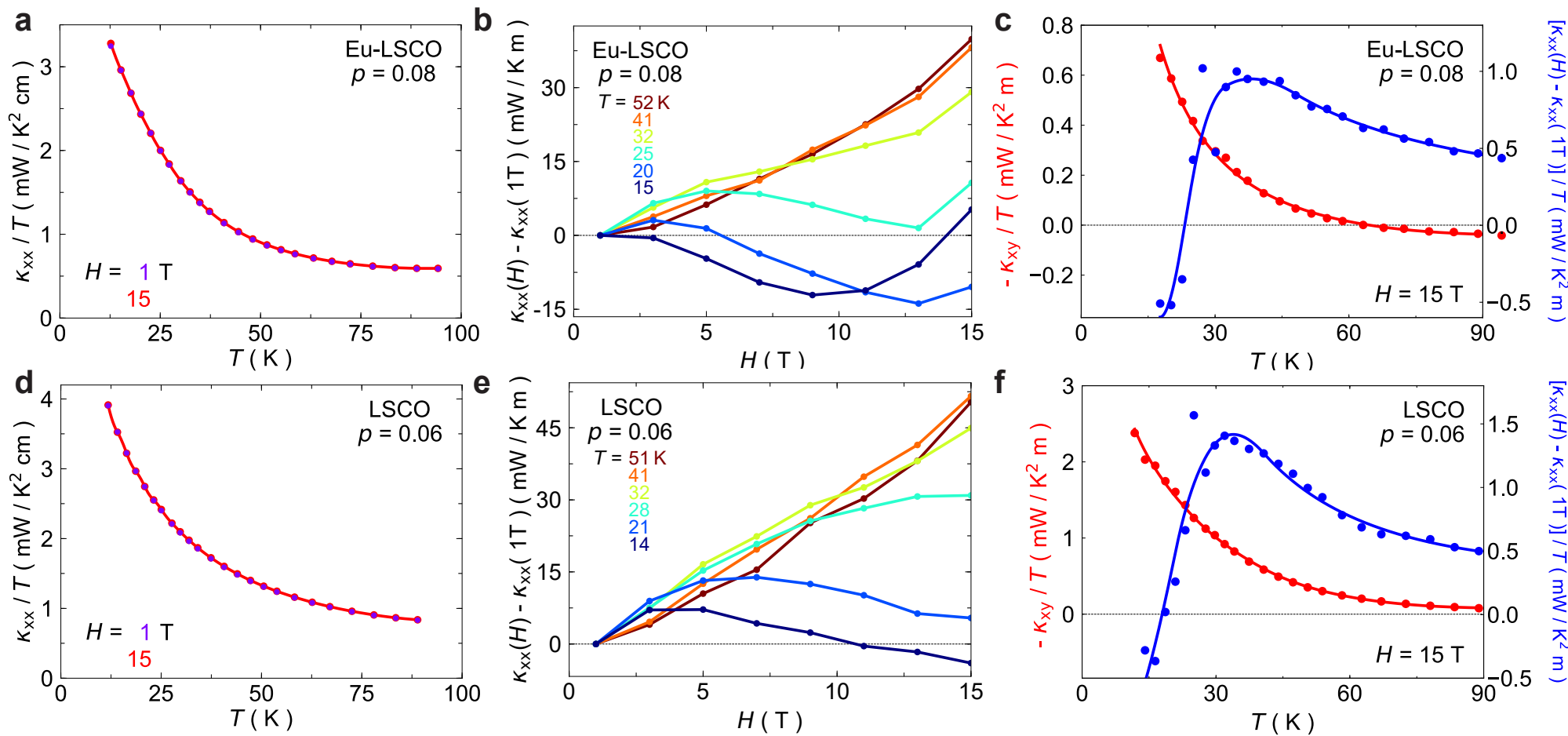


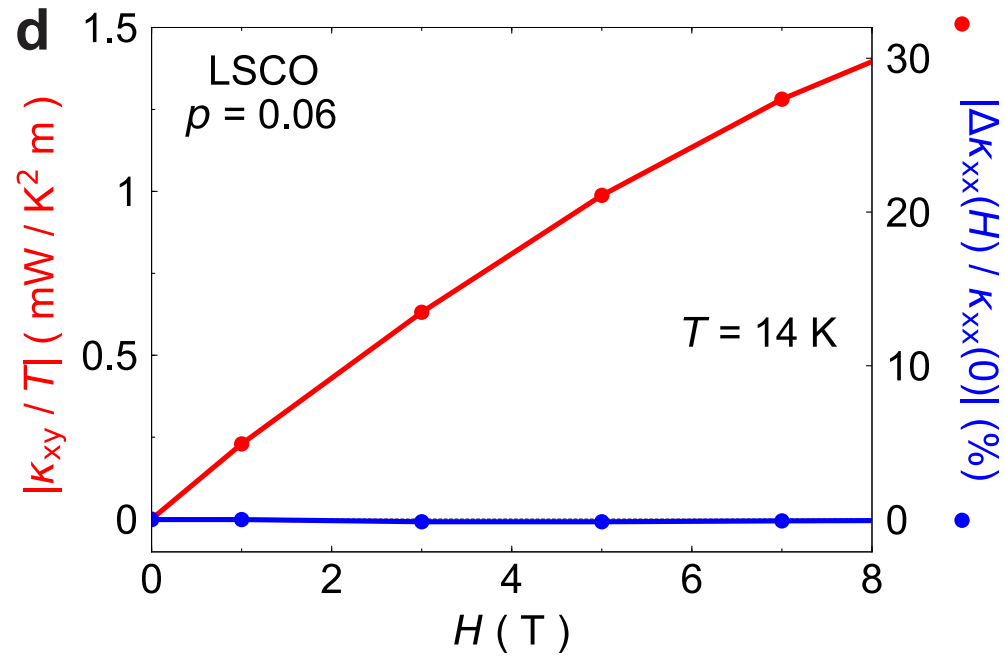
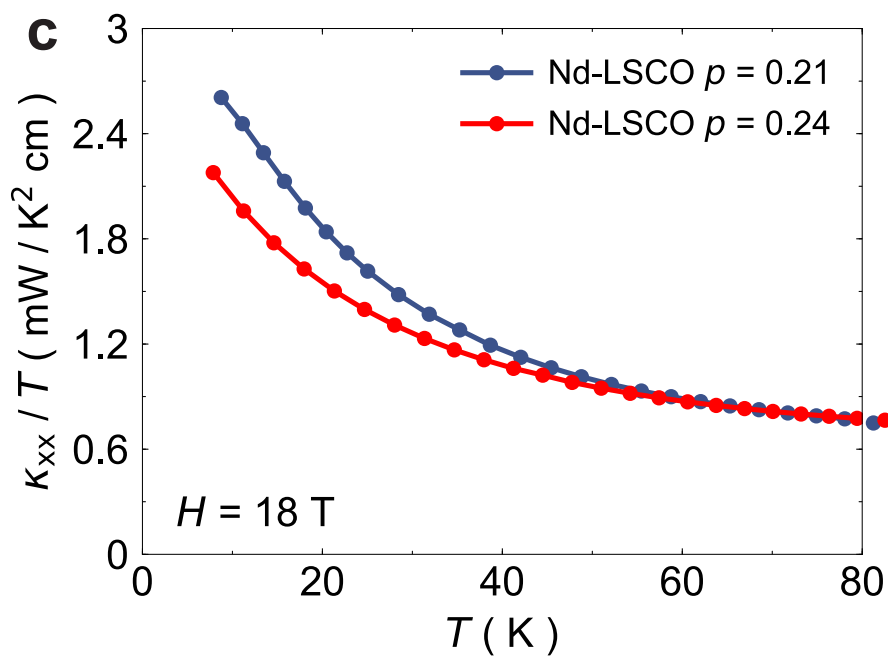
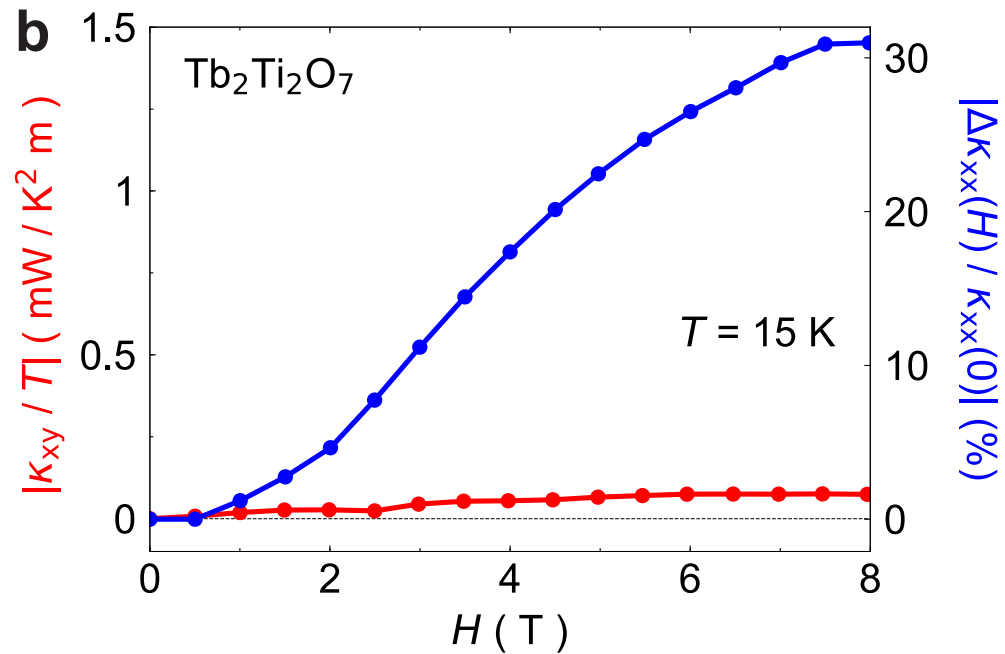
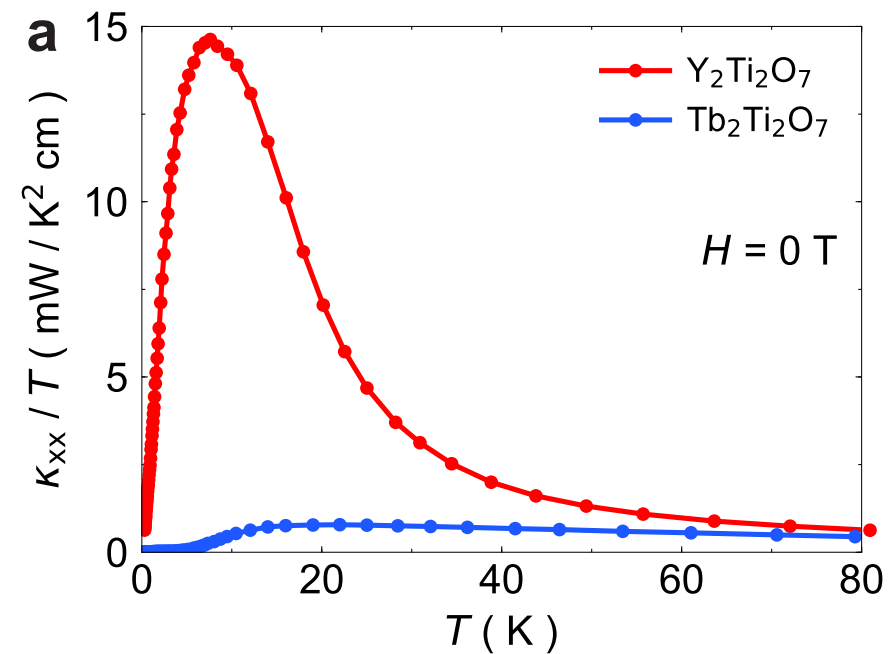
Figure 4



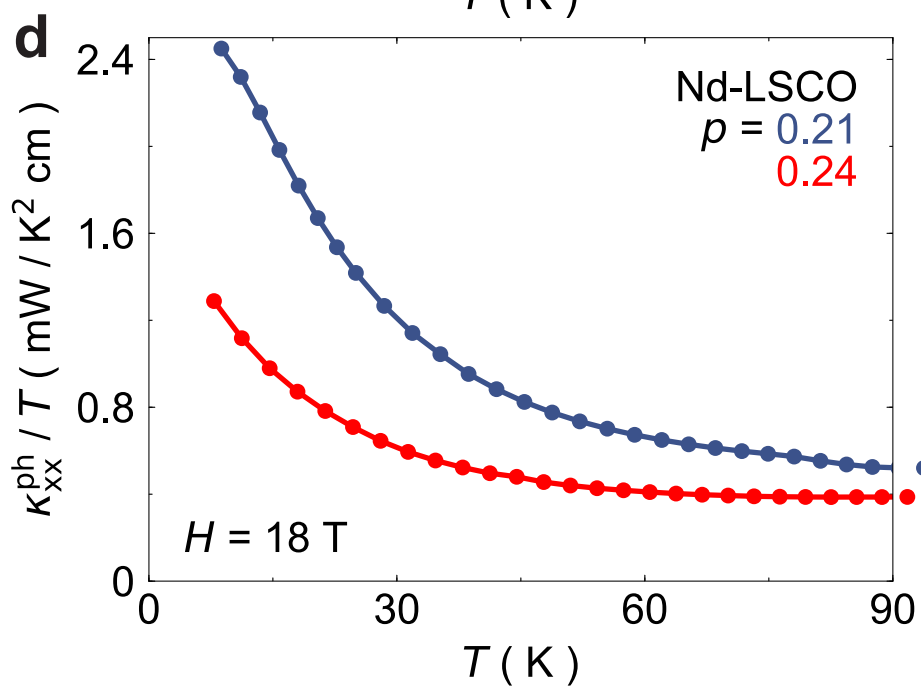
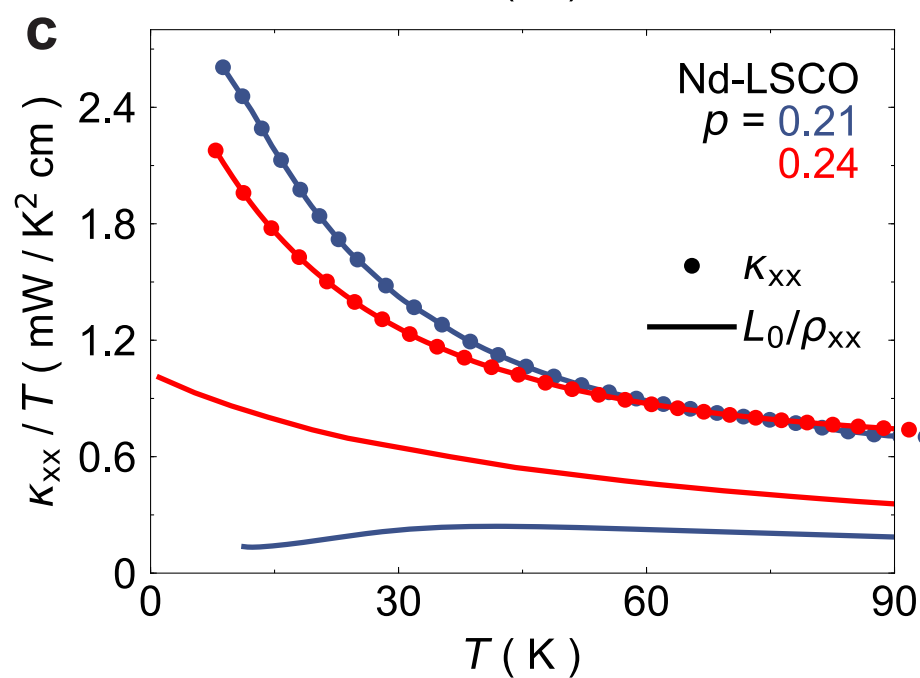
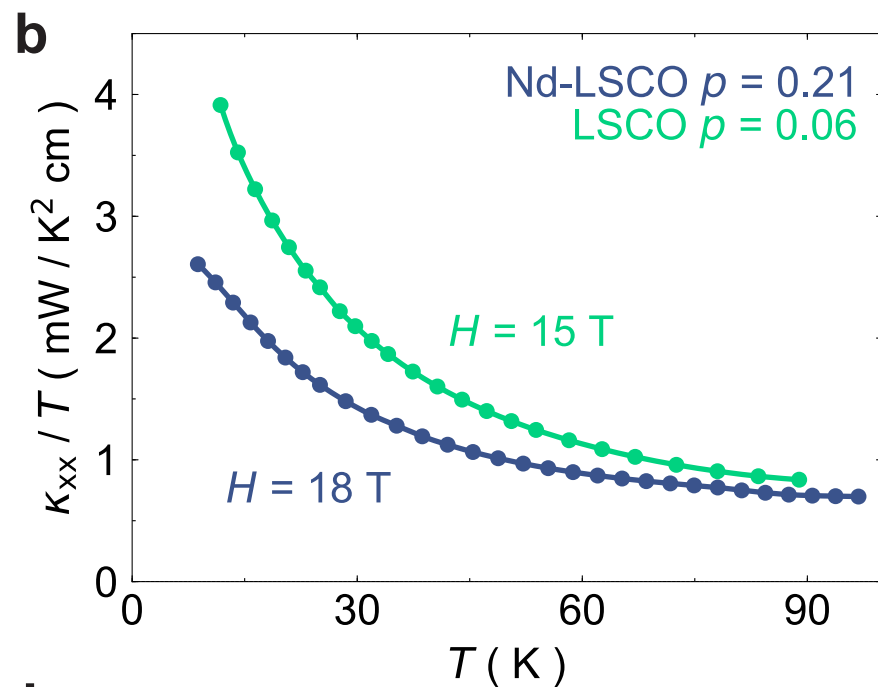
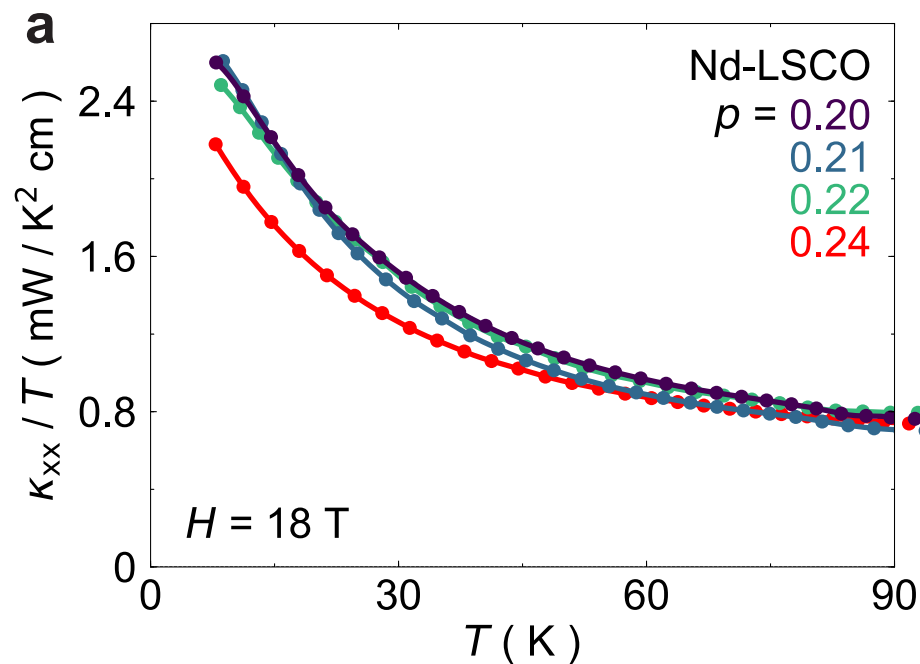
Extended Data Figure 1



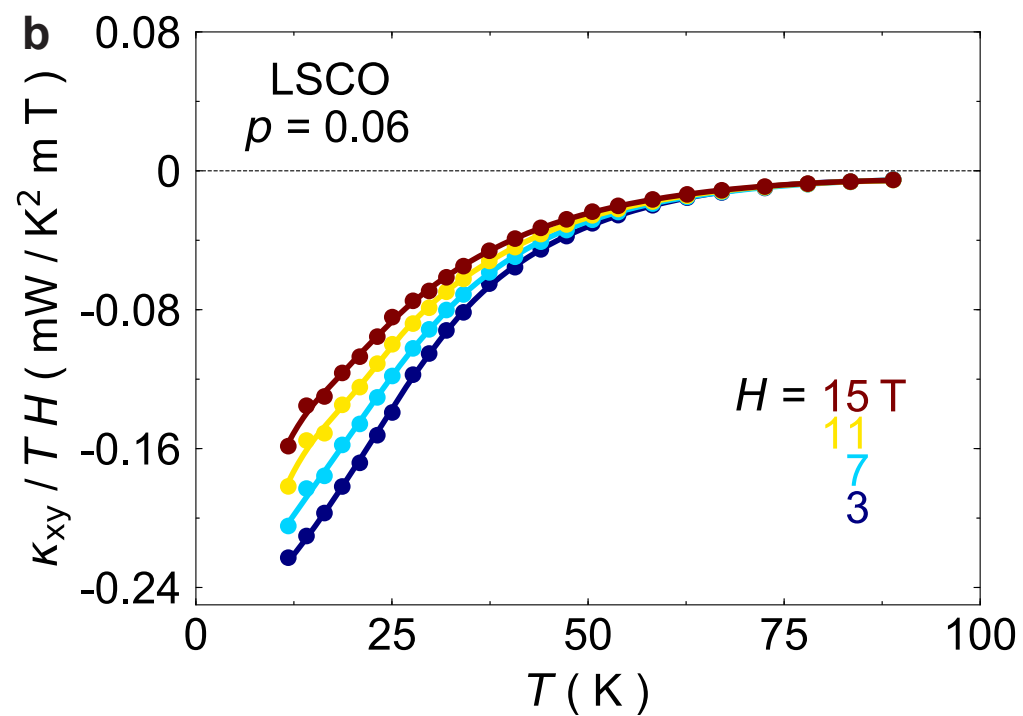
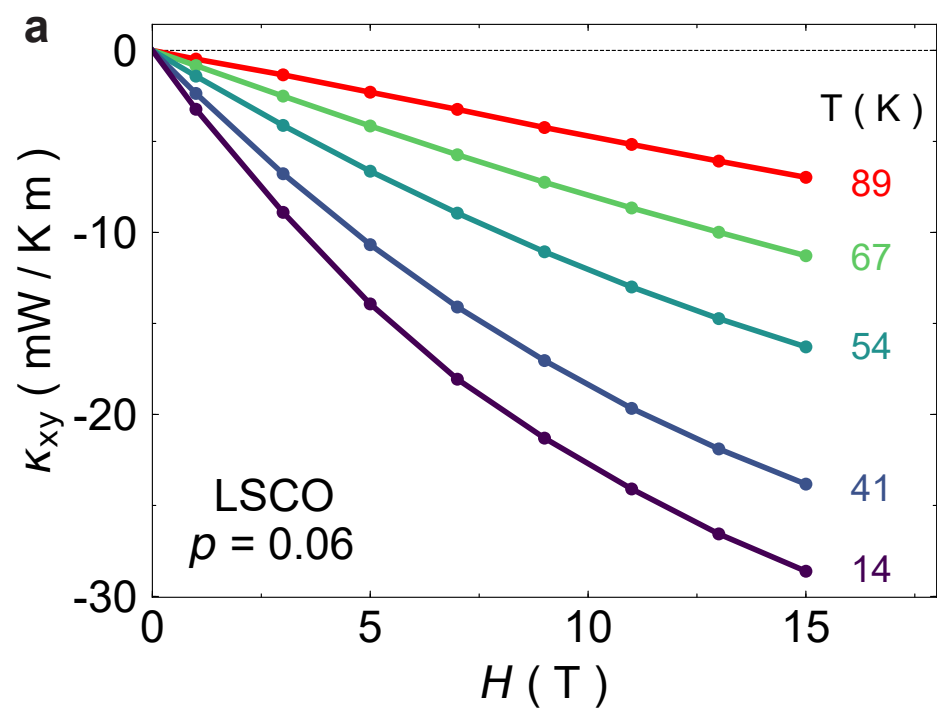
Extended Data Figure 2



Extended Data Figure 3



Extended Data Figure 4



Extended Data Figure 5

